

## Virtual reality framework for editing and exploring medial axis representations of nanometric scale neural structures

Daniya Boges<sup>a</sup>, Marco Agus<sup>b,\*</sup>, Ronell Sicat<sup>c</sup>, Pierre J. Magistretti<sup>a</sup>, Markus Hadwiger<sup>c</sup>, Corrado Calì<sup>d,\*\*</sup>

<sup>a</sup>Biological and Environmental Science and Engineering Division, King Abdullah University of Science and Technology, 23955-6900, Thuwal, Saudi Arabia

<sup>b</sup>Visual Computing Group, Center for Advanced Studies, Research and Development in Sardinia (CRS4), Cagliari, Italy

<sup>c</sup>Visual Computing Center, King Abdullah University of Science and Technology, 23955-6900, Thuwal, Saudi Arabia

<sup>d</sup>Department of Neuroscience "Rita Levi Montalcini", Neuroscience Institute "Cavalieri Ottolenghi", University of Turin, 10043, Turin, Italy.

---

### ARTICLE INFO

#### Article history:

Received April 20, 2020

---

### ABSTRACT

We present a novel virtual reality (VR) based framework for the exploratory analysis of nanoscale 3D reconstructions of cellular structures acquired from rodent brain samples through serial electron microscopy. The system is specifically targeted on medial axis representations (skeletons) of branched and tubular structures of cellular shapes, and it is designed for providing to domain scientists: i) effective and fast semi-automatic interfaces for *tracing* skeletons directly on surface-based representations of cells and structures, ii) fast tools for *proofreading*, i.e., correcting and editing of semi-automatically constructed skeleton representations, and iii) natural methods for interactive *exploration*, i.e., measuring, comparing, and analyzing geometric features related to cellular structures based on medial axis representations. Neuroscientists currently use the system for performing morphology studies on sparse reconstructions of glial cells and neurons extracted from a sample of the somatosensory cortex of a juvenile rat. The framework runs in a standard PC and has been tested on two different display and interaction setups: PC-tethered stereoscopic head-mounted display (HMD) with 3D controllers and tracking sensors, and a large display wall with a standard gamepad controller. We report on a user study that we carried out for analyzing user performance on different tasks using these two setups.

© 2020 Elsevier B.V. All rights reserved.

---

### 1. Introduction

The brain cells, together with their processes, are complex three-dimensional structures, and improving the visual understanding of the relationships between morphological features and functional aspects of these cells is of primary importance to neuroscientists. The recent progress in digital acquisition and

analysis of biological samples, e.g., brain tissues, is offering unprecedented possibilities of insights for neuroscientists. For instance, automated serial section electron microscopy (3DEM) provides electron micrographs that can reach a resolution of a nanometer per pixel, therefore revealing features ranging from full structural cellular details such as axons, dendrites, and synapses (the so called "neuropil"), to smaller intracellular organelles like synaptic vesicles. However, neuroscientists still require effective tools and applications to handle this large and

\*Joint first and corresponding author: magus@hbku.edu.qa.

\*\*Corresponding author: corrado.calì@unito.it

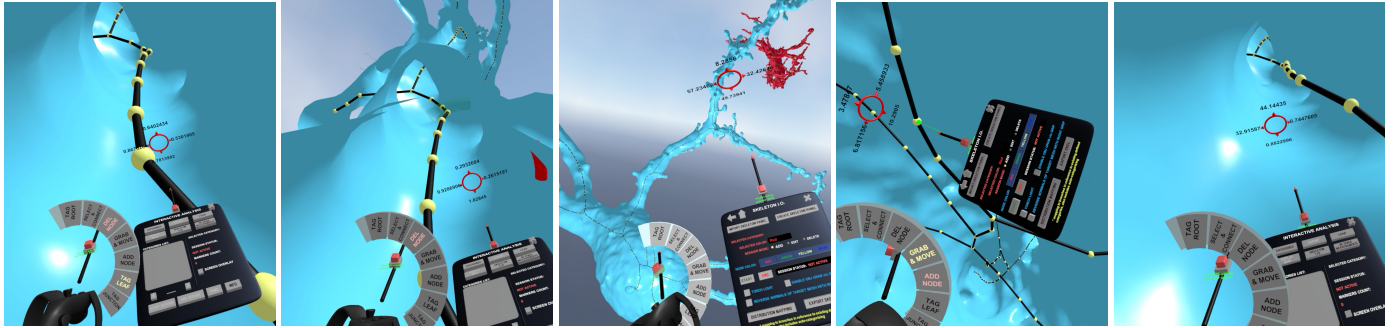


**Fig. 1.** Our proposed virtual environment enables neuroscientists to immersively create, proofread, and explore medial axis representations or skeletons of nanoscale reconstructions of brain cells. In the example scenario above, skeletons are represented as connected nodes (yellow spheres) and edges (black cylinders), while brain cells are depicted as shaded surfaces (using a light blue color in this example).

complex data. Morphology data at nanoscale resolution provide domain scientists fundamental information for understanding neural processes and interaction between cellular structures [1]. Quantifications have particular relevance when extracted data are used to infer parameters allowing mathematical modelization of biological processes [2, 3]. Furthermore, the challenge of making qualitative and quantitative assessments of complex and visually occluded individual cellular structures, or groups of them, is beginning to attract neuroscientists towards the use of immersive visualization paradigms. Hence, during recent years, various laboratories pioneered the use of virtual reality (VR) in supporting electron microscopy (EM) structural analysis [4, 5, 6]. However, previous pipelines were engineered around the need of exploratory analysis of brain structures for specific morphology studies [4], or neuroenergetics investigations [5, 7]. More recently, the need for more efficient extraction of features of branch-based whole cell structures, either for quantification and classification purposes [8], has emerged. Especially neurons, but also glia, can be adequately schematized through skeleton representations, and nowadays, various laboratories are investing important resources on creating faithful and smooth medial axis representations of brain cells. These skeleton representations can be used for various kinds of novel visual and statistical analysis. To this end, time consuming image-based manual tools [9, 10, 11] are commonly used for tracing neural processes on confocal images. More complicated automatic methods for recovering medial axis representations on nanometric scale electron microscopy stacks exist but are

still in their infancy [12] and not yet routinely used for processing brain cells.

In this paper, we present a novel VR-based framework targeted on creating, proofreading, and exploration of skeleton-based representations of nanoscale brain cells surface reconstructions. The system integrates the following components:

- fast servo-assisted semi-automatic methods for creating skeletons of complex brain cellular reconstructions;
- tools for proof-reading (checking, correcting, comparing) medial axis representations;
- exploration tools, e.g., for performing geometric measurements and statistical computations related to cellular structures and their skeletal representations.

The system is currently used by expert domain scientists for analysis of various cells reconstructed from the somatosensory cortex of a juvenile rat [1]. We report on a preliminary subjective evaluation of the immersive environment performed by domain experts during creation and proofreading of complex medial axis representations, as well as during analysis of organelles distributions. This paper is an extended version of the proceeding contribution presented at Smart Tools and Applications for Graphics conference [13]. We provide here a more thorough exposition, together with a more effective external semiautomatic tracing tool for editing medial axis branches. Moreover, we extended the framework to work in a monocular setup with a large scale display wall, and we carried out a user study for evaluating the performances of the system for creat-

ing and editing skeleton representations, either in the monocular display wall setup and in the stereoscopic HMD-based virtual reality setup. To our knowledge, this is the first interactive system targeted to the creation, proof-reading and analysis of skeleton-based representation of cellular structures, and the preliminary reports of usage by expert and novice users provided us promising indications that these kind of systems can positively effect the way ultrastructural analysis is carried out in neuroscience domain.

## 2. Related work

Our work deals with the application of virtual reality (VR) technologies to neuroscience investigations coupled with the computation of medial axis representations of highly detailed branched cellular brain structures. In the following, we discuss the previous work mostly related to our contribution.

*Virtual reality in neuroscience.* Due to the ubiquity of desktop systems, most commonly used visual analysis tools in neuroscience are designed as desktop applications [14, 15]. However, more recently, there is general consensus that the use of stereoscopic techniques, e.g., in VR systems, can provide a more immersive way to explore brain imaging data [16], and that the increased dimensionality provided by stereoscopy is beneficial for understanding depth in the displayed scenery [17, 18]. With respect to immersiveness, the effect of stereoscopy has been previously evaluated in the context of visual analysis of volume data, particularly for semitransparent volume rendering [19, 20], isosurfaces [21], confocal volume images [22], and for interactive graph analysis [23, 17, 16]. Successful examples of applying VR technologies to neuroscience investigations include analysis of glycogen distribution related to neuronal morphologies [4], systems for exploring connectomes [24], systems for tracing neurons in microscope scans of primates' visual cortex [6], and the use of heat maps for representing absorption probabilities on nanoscale surface reconstructions [5]. Very recently Xu et al. [25] introduced TempoCave, a system for analyzing dynamic brain networks by exploring activity patterns in different regions in the brain, computed by processing

raw data retrieved from functional magnetic resonance imaging (fMRI) scans [25]. In this work, we describe an immersive environment for performing shape analysis that is mainly targeted on skeleton representations of nanometric reconstructions. To our knowledge, it is the first application of a VR environment towards morphological analysis of medial axis representations, particularly of brain cells.

*Skeleton-based representation of surface meshes.* Medial axis representations or skeletons can be considered descriptors which jointly describe the geometry, topology, and symmetry properties of a shape in a compact and intuitive way, providing a means to capture the essence of a 3D shape [12]. Automatically or semi-automatically producing accurate skeleton representations is a challenging task. During the last decades, many techniques have been proposed, particularly by the computational geometry community, for different kinds of 3D models. For a comprehensive discussion of the recent methods for creating 3D medial axis representations, we refer the readers to state-of-the-art reports by Tagliasacchi et al. [12], and by Sobiecki et al. [26]. In general, there is a huge collection of methods to obtain 3D skeletons, which can be classified according to the input representation: mesh-based [27, 28, 29, 30] and voxel-based representations [31]. Since our system is focused on surface representations, we will mostly consider methods that use meshes, even if our system can be considered independent from the method used for obtaining the medial axis representation of the morphology considered. The system has been designed to import skeleton representations coming from different automatic frameworks: for our initial analysis, we considered the Mean Curvature Skeleton (MCS) algorithm [27], and the Center Line Tree method [32], which are implemented in the Avizo [33] framework.

*Medial axis representations in neuroscience.* Since medial axis representations provide an adequate and convenient description for branched structures, recently, neuroscientists started exploiting them for representing complicated cellular structures, especially neurons. To this end, they derived specific metrics

for comparing branched structures, i.e., trees, based on geometrical and topological features [34, 35, 36]. These metrics are then used for investigating differences and analogies between morphologies or in general for performing identification and classification [37, 38, 39]. Following this philosophy, recently Kanari et al. [40] developed a classification framework for neurons completely based on skeletons, which is based on specific topological representations, called persistence diagrams. The framework has been successfully used for objective morphological classification of neocortical pyramidal cells [8]. It has also been integrated into a more general collaborative framework for the analysis and visualization of neuronal morphology skeletons reconstructed from microscopy stacks [41]. Our proposed immersive environment addresses similar needs, and it is customized for the proofreading and analysis of skeletons of different cells, while leveraging the benefits of a VR system. We believe that 3D branched structures derived by brain cell morphologies can be more effectively analyzed by leveraging cues provided by stereoscopy and full immersion which are well suited for 3D scenes. Our framework is general and customizable, and it can be extended to integrate other geometric representations and visual encodings.

### 3. Application domain: morphology analysis in neuroscience

Before detailing the proposed immersive environment, we first provide a brief description of our particular application domain in neuroscience: the ultrastructural investigation of brain cellular morphologies at nanometric scale.

*Ultrastructural analysis.* Neuroscientists often perform ultrastructural analysis of brains samples through ex-vivo digital acquisition of very small brain portions. To this end, they use high resolution electron microscopy systems equipped with high precision cutters [42]. Through this methodology, domain scientists get 3D 8bit image stacks containing cellular membranes at nanometric resolution (see Fig. 2 left). These datasets allow them to visually individuate and annotate cellular and molecular features, such as compounds, synapses, and organelles like mi-

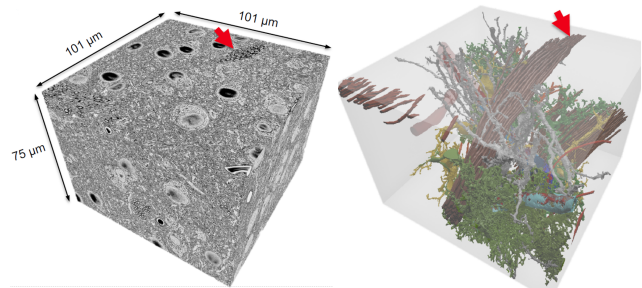


**Fig. 2. Data preparation.** Left: we tested the proposed immersive system on models reconstructed from an image stack acquired by serial electron microscopy of a sample from a juvenile rat's somatosensory cortex. Right: sparse reconstruction provides high resolution surface representation of full cellular morphologies.

ochondria, vesicles and endoplasmatic reticulum (ER). Nowadays, EM imaging technique is becoming increasingly popular in the field of connectomics, since it enables accurate reconstructions of the connections between neurons [43].

*Processing pipeline.* Given a 3D stack of images acquired by an electron microscope (Fig. 2 left), neuroscientists need to pass through different processing tasks in order to extract relevant 3D shape representations of cellular structures, in form of surface meshes (Fig. 2 right), that can be used for statistical computations, simulation, or rendering. The processing pipeline consists of carrying out dense or sparse reconstructions, by using manual, semiautomatic or automatic tools, which label the image pixels in the stack, i.e., assigning them with a unique object identifier for the various structures of interest, such as neural axons, dendrites, organelles, nuclear envelopes, etc. In this work, we used a hybrid two-step pipeline [44], composed by:

- a rough automatic segmentation performed offline through the iLastik tool [45], for finding the gross features and processes of a cell
- a manual proofreading phase, performed through the TrackEm2 tool [46], for specifying exact object boundaries and finer details.

*Morphology features.* Once the various cells and sub-parts are labelled on a per-pixel level in the image stack, neuroscientists perform various ultrastructural analyses by studying the morphology of the following biological structures (Fig. 2 right):

209 • **Neurons:** composed of *axons* and *dendrites*, which are<sup>244</sup>  
 210 the terminals respectively sending and receiving electric<sup>245</sup>  
 211 signals through *boutons* and *spines*. Boutons and spines<sup>246</sup>  
 212 are linked and form *synapses*.<sup>247</sup>

213 • **Glial cells:** neuroscientists mainly focus on *astrocytes*,<sup>248</sup>  
 214 which are metabolically involved in feeding neurons, *mi-*<sup>249</sup>  
 215 *croglia*, which are the main form of active immune defense<sup>250</sup>  
 216 in the central nervous system by acting as macrophages,<sup>251</sup>  
 217 and *oligodendrocytes*, which produce the myelin sheath<sup>252</sup>  
 218 insulating neuronal axons.<sup>253</sup>

219 • **Organelles:** domain scientists mainly focus on *mitochon-*<sup>254</sup>  
 220 *dria* and *endoplasmatic reticulum*, which are contained in<sup>255</sup>  
 221 axons, dendrites, and glial cells. They contain the machin-<sup>256</sup>  
 222 ery for chemical transformations.<sup>257</sup>

223 Neuroscientists are interested in studying the relationships<sup>259</sup>  
 224 between the aforementioned structures, and perform geomet-<sup>260</sup>  
 225 ric analysis for recovering parameters to be used for simulation<sup>261</sup>  
 226 purposes or for classification [40, 47].<sup>262</sup>

227 *Medial axis representations.* Most of the considered cells have<sup>263</sup>  
 228 complicated branching structures, which are very difficult to an-<sup>264</sup>  
 229alyze using standard mesh representations (see Fig. 2 right). To<sup>265</sup>  
 230 this end, skeleton representations provide an effective tool for<sup>266</sup>  
 231 describing them and classifying the various branches, according<sup>267</sup>  
 232 to the size and the branching level, starting from the soma. For<sup>268</sup>  
 233 this reason, neuroscientists are increasingly focusing on tech-<sup>269</sup>  
 234 nologies that can support them in recovering accurate skeletal,<sup>270</sup>  
 235 representations [35, 8].<sup>271</sup>

## 236 4. System overview

237 The proposed system is a standard 3D framework customized<sup>274</sup>  
 238 to be used with a stereoscopic HMD-based setup using room<sup>275</sup>  
 239 scale tracking technology (VR), or with a large screen display<sup>276</sup>  
 240 for collaborative sessions. In VR, the system allows the user<sup>277</sup>  
 241 to interact with a 3D environment through two motion-tracked<sup>278</sup>  
 242 hand-held controllers, i.e., by pointing/selecting objects, or se-<sup>279</sup>  
 243 lecting motions through menus. When working with the display<sup>280</sup>

wall, a generic gamepad controller can be used for input. The framework was developed on top of the Unity game engine.

*Scene representation and rendering.* The immersive environment provides real-time exploration of scenes composed of surface representations of brain cells and schematic representations of the associated medial axes or skeletons. The level of transparency of surfaces can be interactively controlled in a way to provide context for skeleton exploration. Since the system is also designed for providing endoscopic analysis of cellular processes, a torch tool is provided for shading mesh walls and dark corners during exploration. The tool is attached to one of the manipulators and can be easily used to illuminate dark areas. Basic 3D manipulation options are provided, e.g., object scaling and placement, as well as material and color assignment. Moreover, users can flip the mesh normals, in a way to have a more convenient way of examining the inner/outer mesh surfaces. With respect to skeletons, the system uses three different representations:

- **sprite-based:** 2D line segments/ribbons represent the whole skeleton geometry (implemented using Unity line renderer module);
- **node-based:** only spheres represent skeleton nodes; depending on the skeleton data, the system can utilize only primary nodes to provide a rough representation of skeletons;
- **complete:** skeleton nodes are represented by spheres while skeleton edges are represented by cylinders.

*Main features.* After loading the cellular morphology, the system enables users to operate on medial axis representations in two modes: *create mode* for creating skeletons from scratch, and *proofread mode* for correcting/editing previously computed skeletons. In proofread mode, the system requires that previously computed medial axes respect specific notations represented in table 1. This notation is valid for most graph representations and is widely used by many graph processing software. Specifically, in this paper, we focused on skeletons computed through three methods:

Algorithm/Tool	Notation/ File Format	Data Type
Centerline Tree (Avizo)	[ Point ID , Thickness , X Coord , Y Coord , Z Coord ]/ .CSV [ Segment ID , Node ID1, Node ID2, Point IDs List ] / .CSV	Points (file1) Branches(file2)
Mean Curvature Flow	[ x, y ,z ] / txt [ NodeID1, NodeID2 ] / .txt [ Sum of points(n) , X, Y, Z, Xn,Yn,Zn ] / .txt	Points (file1) Branches (file2) Points and Branches
Simple Neurite Tracer (Fiji)	[ NodeID, Cell Type , X, Y, Z, radius, ParentID ]/.SWC	Points with Branches

Table 1. Notations/formats used for skeleton data.

- an automatic volume-based method [32], implemented in the Avizo framework [33] - it uses connected components for graphs, combining a union-find and a recursive algorithm;
- an automatic mesh-based method [27] - it uses iterative contraction through mean curvature flow evolution;
- a manual image-based tracer implemented in the Fiji system [10].

The system provides support for importing and exporting standard skeleton file formats that are compatible with the previously mentioned systems. It can also be easily extended to support other formats/notations.

## 5. Interactive tools

The proposed system provides interactive tools for editing/manipulating medial axis representations. We describe available interactions using 3D controllers for VR as well as for gamepad controllers for the display wall. We tried to keep most interactions similar for the two controllers in order to reduce the effort for users in terms of switching between the two if necessary. In the following, we discuss interactions based on 3D controllers but the same applies to a gamepad with the trigger button corresponding to gamepad buttons with pre-mapped

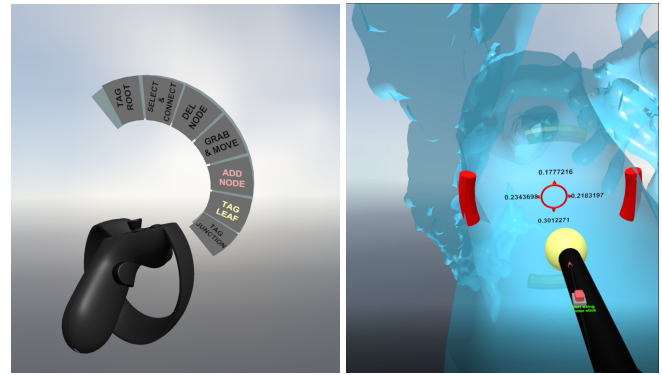


Fig. 3. Interactive tools. Left: an arch-shaped menu attached to the left controller allows users to select interaction mode with skeletons. Right: a stabilizer servo-assisted tool (in red) guides users through the process of skeleton branch tracing.

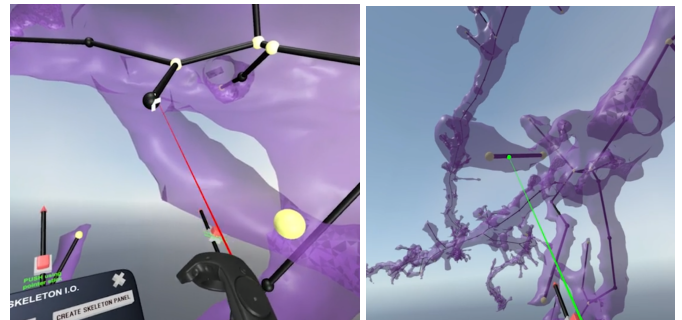


Fig. 4. Skeleton editing. Our system provides effective tools for rapid editing of skeleton branches. Left: adding connection between nodes. Right: removing a wrong edge from a skeleton branch.

functions, and 3D pointing corresponding to using the gamepad arrow and analog buttons to move the camera and the pointer. The core interactions are summarized in 7 options laid out in an arch-shaped menu (see Fig. 3 left), attached to the left 3D controller. The user can choose one of the options by first rotating his/her wrist between 0 and 180 degrees, and then, once settled on an option, pressing the trigger buttons to select. The options provided by the system are the following:

- **Add Node:** using the trigger button, the user can create a node in 3D space. This process can be fully manual or controlled by a servo-assisted stabilizer. Upon creation, the system automatically pairs up nodes with each other and connects them with an edge, hence, creating a single connected path;
- **Grab and Move:** as part of the proofreading/editing process, nodes can be moved anywhere simply by grabbing them and moving them. This can be achieved thru a com-

320 bination of an action grab initiated by pressing and holding  
 321 of the controller's *grip* button while touching the surface  
 322 of the target node;

- 323 • **Select and Connect:** using a combination of point  
 324 and trigger click, the user can select two nodes subse-  
 325 quently and the system creates an edge connection be-  
 326 tween them (see Fig. 4 left);

- 327 • **Delete Skeleton Element:** the system allows the right  
 328 controller to shoot a laser pointer by pressing on the con-  
 329 troller touch pad. The user can then delete nodes and edges  
 330 by pointing at a valid skeleton unit object followed by a  
 331 trigger button click (see Fig. 4 right);

- 332 • **Tag Root, Junction, and Leaf:** a similar action of point  
 333 and trigger at a specified node will save it in its correspond-  
 334 ing skeleton file as one of these values: 0=Root, 1=In-  
 335 ternal, 2=Leaf, 3=Junction. Tagging a node with "Leaf",  
 336 "Junction", or "Root" marks it with a special color mate-  
 337 rial and finalizes the current path as a single branch.

- 338 • **Undo:** an action that saves users the troubles of having  
 339 to delete a mistake node manually, and instead, they can  
 340 revert to multiple steps back during the skeleton creation  
 341 process.

342 *Path stabilizer: tunnel metaphor:* The system provides a semi-  
 343 automatic method for creating skeleton branches through one of  
 344 the VR input controllers. This method is built around a visual  
 345 user guide, that operates as reference when tracing the tunnel-  
 346 like cellular processes through endoscopic navigation. During  
 347 the exploration of the process, a path stabilizer transparently  
 348 and automatically places skeleton nodes in the middle of the  
 349 process section. The automatic node position computation is  
 350 performed by shooting straight rays onto a number of radial  
 351 directions, and computing the average distance to the surround-  
 352 ing wall boundaries. This simple but effective method provides  
 353 a way to rapidly trace main cellular processes, and create fully  
 354 controlled skeleton representations. In current implementation  
 355 we use 16 rays for computing the average distance.

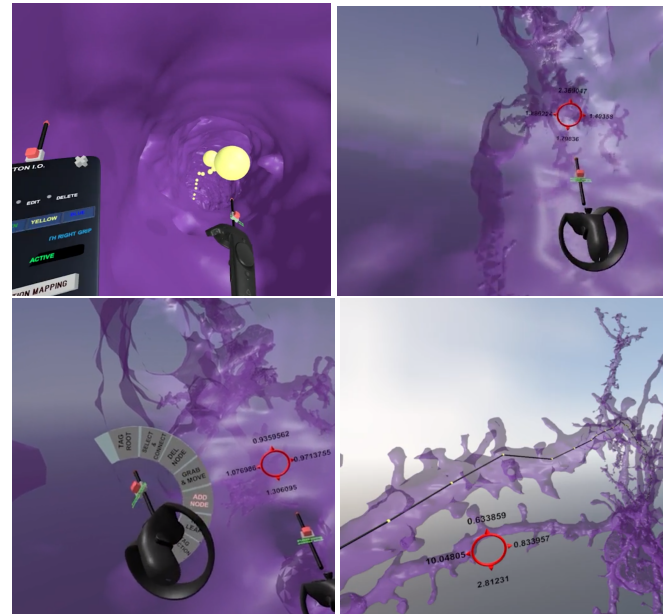


**Fig. 5. Skeleton creation.** We propose a semiautomatic and guided method for creating skeletons, based on endoscopic exploration of cell branches, and using a servo-assisted stabilizer.

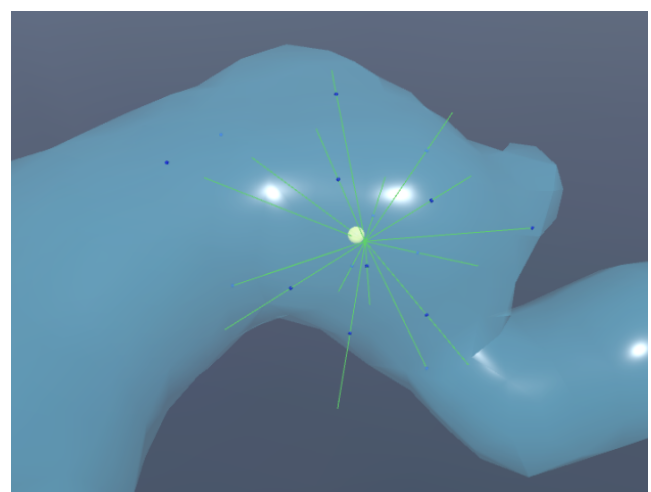


**Fig. 6. External tracing.** Users can trace branches through external 3D pointing, since a semiautomatic algorithm computes running barycenters through multiple iterative ray casting.

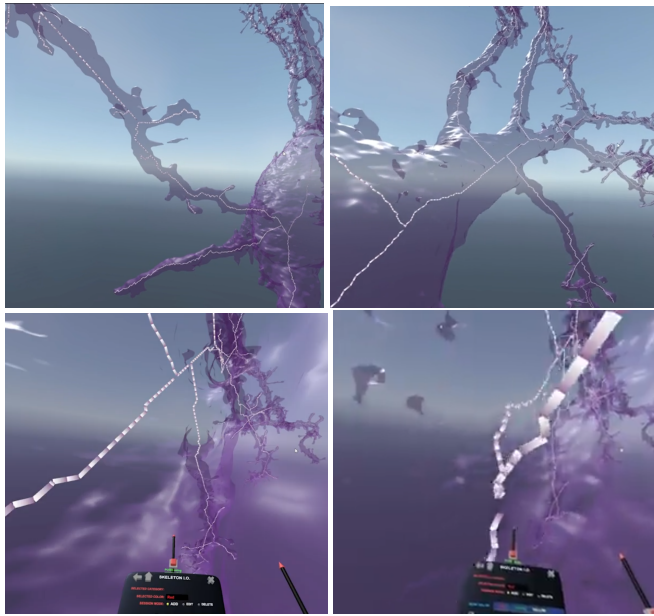


**Fig. 7. Skeleton proofreading.** Our system enables domain scientists to perform effective proofreading of skeletons by using endoscopic and external metaphors.

<sup>356</sup> *Path stabilizer: tracing metaphor.* In order to speed up the trac-<sup>382</sup>  
<sup>357</sup> ing process of long branches exhibiting low curvature, like it<sup>383</sup>  
<sup>358</sup> happens for some neural dendrites and axons, we introduced a<sup>384</sup>  
<sup>359</sup> semi-automatic external tracing metaphor. With this tool, user<sup>385</sup>  
<sup>360</sup> is able to follow the path of the specific through 3D pointing,<sup>386</sup>  
<sup>361</sup> while the system uses ray casting for intersecting the branch,<sup>387</sup>  
<sup>362</sup> and, starting from the ray, an iterative approach shoots different<sup>388</sup>  
<sup>363</sup> rays similarly to the previously described tunnel metaphor. In<sup>389</sup>  
<sup>364</sup> order to accelerate the computation of nearest neighbors, we use<sup>390</sup>  
<sup>365</sup> a KD-tree data structure. The running barycenters of the differ-<sup>391</sup>  
<sup>366</sup> ent ray intersections are added as nodes in the current skeleton<sup>392</sup>  
<sup>367</sup> branch. Even in this case, in current implementation we use 16<sup>393</sup>  
<sup>368</sup> rays for computing the running barycenter. This method proved<sup>394</sup>  
<sup>369</sup> to be very fast and effective for processes not exhibiting sharp<sup>395</sup>  
<sup>370</sup> features and bumps (see section 7). Figure 6 shows an example<sup>396</sup>  
<sup>371</sup> of the algorithm for computing a node.

## 372 6. Setup and dataset

<sup>373</sup> Our proposed immersive system is used by neuroscientists<sup>400</sup>  
<sup>374</sup> for performing real-time creation, proofreading/editing, and ex-<sup>401</sup>  
<sup>375</sup> ploration of brain cell reconstructions based on medial axis rep-<sup>402</sup>  
<sup>376</sup> resentations.

Machine	OS	Task	Specs
Asus ROG G703G	Windows 10 Pro	Immersive environment	32GB DDR4, Intel Core i9-8950HK 4.8 GHz, Nvidia GTX 1080 8GB GDDR5X, 2X 256GB PCIE SSD + 2TB SSHD FireCuda.
Supermicro	Linux CentoS 7	Data processing and skeleton creation	1TB memory, Intel(R) Xeon(R) Gold 6150 CPU2.70GHz (18 Cores), Nvidia GK104GL Quadro K5000, N/A

**Table 2. Machines used for immersive environment and data preparation.**

<sup>377</sup> *Implementation details.* The immersive system has been de-<sup>382</sup>  
<sup>378</sup> veloped and deployed using the Unity game engine (version<sup>383</sup>  
<sup>379</sup> 5.6.3, via C# scripting). For VR, it uses SteamVR and the<sup>384</sup>  
<sup>380</sup> VRTK software packages [48], which provide smooth immer-<sup>385</sup>  
<sup>381</sup> sive system-user interaction as well as cross-hardware setup<sup>386</sup>  
<sup>382</sup> compatibility. In this way, the same application can be used<sup>387</sup>  
<sup>383</sup> on various VR setups, like Oculus Rift [49] or HTC Vive [50].<sup>388</sup>  
<sup>384</sup> For computing automatic skeletons, and for other preprocessing<sup>389</sup>  
<sup>385</sup> tasks, we implemented and used C++ applications and Python<sup>390</sup>  
<sup>386</sup> scripts. In addition, we used Avizo (a commercially available<sup>391</sup>  
<sup>387</sup> data analysis/visualization software framework) for computing<sup>392</sup>  
<sup>388</sup> high-quality skeletons, and preprocessing was carried out on a<sup>393</sup>  
<sup>389</sup> workstation equipped with two CPUs of 10 cores each (see<sup>394</sup>  
<sup>390</sup> table 2 for additional details).

<sup>395</sup> *Data preparation.* For testing purposes, we considered five<sup>396</sup>  
<sup>396</sup> complex cellular structures reconstructed from a p14 rat<sup>397</sup>  
<sup>397</sup> somatosensory cortex. We selected different kinds of cells to show<sup>398</sup>  
<sup>398</sup> different levels of complexity: two neurons, two microglia,<sup>399</sup>  
<sup>399</sup> and one astrocyte [1]. The cells were reconstructed from a<sup>400</sup>  
<sup>400</sup> high-resolution EM stack with approximated size of  $100\mu\text{m} \times$ <sup>401</sup>  
<sup>401</sup>  $100\mu\text{m} \times 76.4\mu\text{m}$  (see Fig. 2 left). The reconstruction process<sup>402</sup>  
<sup>402</sup> was performed through a semiautomatic process [44] involving<sup>403</sup>  
<sup>403</sup> customized components and public domain software like<sup>404</sup>  
<sup>404</sup> iLastik [45] and TrakEM2 [46]. The output of the reconstruc-<sup>405</sup>  
<sup>405</sup> tion process is a series of high resolution triangular meshes re-<sup>406</sup>  
<sup>406</sup> presenting the cellular morphologies (see Fig. 2 right). Further-<sup>407</sup>  
<sup>407</sup> more, each cell was optimized in a way to be watertight and<sup>408</sup>

Name	Picture	Vertices	Time	Before cleaning	Nodes-Edges-Branch	After cleaning	Nodes-Edges-Branch
Neuron1		49,628	10.00		1569— 1573— 201		1318— 1321— 25
Neuron2		78,215	15.28		1,619— 1,629— 357		1215— 1223— 20
Microglial1		48,015	09.00		1,463— 1,479— 165		1443— 1456— 62
Microglia2		125,532	13.53		2,105— 2,122— 260		2060— 2077— 111
Astrocyte		211,004	25.16		4,055— 4,137— 854		3906— 3983— 296

**Table 3. Morphologies and Mean Curvature Skeletons (MCS) of 5 biological cells.** Cells are computed automatically through [27] and proofread and cleaned through our Virtual Reality system. Together with pictorial representations, we report on cell sizes, total times for proofreading and cleaning, and skeleton statistics.

without non-manifold edges and vertices, and in a way to pre-<sup>441</sup>  
 serve all important morphological features. To this end, we used<sup>442</sup>  
 public domain mesh processing tools like Blender [51], Mesh-<sup>443</sup>  
 lab [52], and Ultralizer, a geometry processing tool contained<sup>444</sup>  
 inside the suite NeuroMorphoVis [41]. For getting automatic<sup>445</sup>  
 medial axis representations of the considered morphologies, we<sup>446</sup>  
 used the Mean Curvature Skeleton algorithm [27], as well as<sup>447</sup>  
 the Centerline Tree module both available in Avizo [32]. In<sup>448</sup>  
 table 3 we report on the cell morphologies and the associated<sup>449</sup>  
 skeleton representations. Specifically we provide visual repre-<sup>450</sup>  
 sentations of the morphologies, together with information about<sup>451</sup>  
 their shapes and sizes in terms of vertex counts, visual repre-<sup>452</sup>  
 sentations of automatic skeletons, and skeleton graph statistics<sup>453</sup>  
 (number of nodes, number of edges, and number of branches).<sup>454</sup>

*Hardware setups.* We tested the VR application on a gaming<sup>453</sup>  
 laptop equipped with an Nvidia GTX 1080 8GB GDDR5X<sup>454</sup>  
 GPU. We used the laptop to drive two different display se-<sup>455</sup>  
 tups (see figure 8):<sup>456</sup>

- a stereoscopic immersive Head Mounted Display (HMD)<sup>457</sup>  
 Oculus Rift S [53] with sensors embedded in a way to<sup>458</sup>  
 lower the bulkiness of the system and increase portabil-<sup>459</sup>  
 ity. The display uses a single fast-switch LCD panel with<sup>460</sup>  
 a resolution of  $2560 \times 1440$  with a refresh rate of 80 Hz,<sup>461</sup>  
 field of view of 110 degrees on a workspace of 3.5 meters  
 $\times 3.5$  meters;<sup>462</sup>
- a monocular collaborative large-scale display wall com-<sup>463</sup>  
 posed of an array of tiled  $3 \times 4$  Narrow Bezel Monitors<sup>464</sup>  
 $(55")$  ( $7680 \times 3240$  pixels) for a total resolution of around<sup>465</sup>  
 25 Mpixels. For the monoscopic display setup, the Oculus<sup>466</sup>  
 Rift input devices were substituted by an Xbox gamepad<sup>467</sup>  
 controller.<sup>468</sup>

The two different setups provide different working environment<sup>470</sup>  
 in which the tools can be used as direct pointers for perform-<sup>471</sup>  
 ing editing operations on the scene. The proposed interacting<sup>472</sup>  
 metaphors are general and can be adapted to different setups,<sup>473</sup>  
 using different kind of controlling devices, like touch devices or<sup>474</sup>  
 gestures [54]. According to the taxonomy presented by Mendes<sup>475</sup>

et al. [54], the considered setups are the following: an immersive one, with 3D controllers physically providing a direct metric control over the scene represented in a virtual workspace, and a gaming one, with gamepad controllers controlling a 2D display wall, in an indirect way. Regarding the design choices, we decided to do not use the same controllers in both setups since the oculus controllers are natively connected to a real 3D physical setup, and we believe they would not be naturally understood if coupled to a monoscopic display setup.

## 7. Results

We carried out a preliminary assessment of the system to understand how is the usability in the context of exploratory analysis of different kind of cells. We report here on two kind of evaluations: a subjective qualitative assessment performed by expert users on complete creation of skeleton representations of entire cells, and an user study for evaluating the performance of the system for editing tasks either in HMD-based stereoscopic setup and Wall-based monoscopic setup. Finally we report on a use case for measurement analysis on distributions of branched-like organelles.

### 7.1. Expert evaluation

A preliminary evaluation of the system was performed by two expert neuroscientists on cells of table 3. Domain scientists were particularly interested in obtaining accurate and clear skeletal representations to be used as descriptors of highly intricate cellular structures. In general, they want to have precise control of medial axis representations, in a way to be able to clearly separate main processes from fine details that have different biological meaning (for example dendritic shafts and spines in neurons). In this sense, most automatic systems provide "dirty" medial axis representations, thus we expected that an interactive tool helping in cleaning skeletons would receive a positive feedback. Moreover, we expected that the immersiveness provided by virtual reality could improve the creation and editing process.



**Fig. 8.** Display setup for user study. We evaluated the system performance under different display conditions: large scale monoscopic display (left), and head mounted stereoscopic display (right).

Cell Name	Skeleton	Time Stereo Int	Time Stereo Ext	Time Mono Int	Time Mono Ext	Nodes—Edges—Branches
Neuron1		25:13	14:24	29:55	25:28	481—480—25
Neuron2		30.50	14:35	22:54	24:11	629—628—20

**Table 4.** Statistics on skeletons generated semi-automatically from scratch for Neuron1 and Neuron2 morphologies.

Cell Name	Algorithm	Nodes—Edges—Branches
Neuron1	MCS	1,569 — 1,573 — 201
	CLT	7,719 — 7,328 — 361
Neuron2	MCS	1,619 — 1,629 — 357
	CLT	9,655 — 9,530 — 516

**Table 5.** Neuron1 and Neuron2 skeleton properties as generated via Mean Curvature Skeleton (MCS) and Centerline Tree (CLT) algorithms.

476 *Skeleton creation from scratch.* Neuroscientists used the sys-  
477 tem for creating skeletons from scratch on two neural mor-  
478 phologies. In table 4, we show statistics about the skeleton cre-  
479 ation process, with different tracing metaphors (internal and ex-  
480 ternal) and different display setups (VR-based and Wall-based).  
481 The procedure consisted of exploring the surface models in or-  
482 der to select the main processes, and trace the branches from  
483 inside the cells, i.e., similar to an endoscopic navigation/view.  
484 Domain scientists felt comfortable in recognizing main pro-  
485 cesses, e.g., dendrites and spines, in a way to correctly trace  
486 the medial axis of interest. Moreover, they felt quite comfort-  
487 able with the path stabilizer, which reduced the number of input  
488 actions on controllers. A comparison of creation times between  
489 the two different display setups and the different tracing inter-  
490 faces shows that expert users were faster when using external  
491 tracing metaphor with stereoscopic VR setup (almost 2X with  
492 respect to the worst case according timings in table 4).  
493

496 tons automatically computed through Mean Curvature Flow  
497 (MCS [27]), and Centerline Tree (CLT [32]). They concluded  
498 that both the methods considered were able to cover all the  
499 morphology features of interest. However, skeletons produced  
500 by CLT appeared to be too highly detailed, with a number of  
501 wrongly assigned branches as well as disconnected parts. Ta-  
502 ble 5 shows the difference in the total number of branches,  
503 nodes and edges for each algorithm for all five cells. In gen-  
504 eral, domain scientists found that skeletons produced by MCS  
505 algorithm contained a lower number of artifacts. For this rea-  
506 son, in all considered cases, they preferred to perform editing  
507 and cleaning on skeletons computed through MCS algorithm.  
508 To this end, they carried out a series of checks depending on  
509 the type of cell, and on the biological significance of the vari-  
510 ous features:

- Identify main branches by tagging their nodes as either leaf, end of branch, or internal nodes. The system identifies all node types based on the degree of each one in the graph tree. However, some needs to be adjusted based on the cell's biological features. Using the VR interactive menu, the user points at a node with the VR controller's laser pointer and then clicks on the trigger button to tag it.

511  
512  
513  
514  
515  
516  
517  
518  
519  
520  
521  
522  
523  
524  
525  
526  
527  
528  
529  
530  
531  
532  
533  
534  
535  
536  
537  
538  
539  
540  
541  
542  
543  
544  
545  
546  
547  
548  
549  
550  
551  
552  
553  
554  
555  
556  
557  
558  
559  
560  
561  
562  
563  
564  
565  
566  
567  
568  
569  
570  
571  
572  
573  
574  
575  
576  
577  
578  
579  
580  
581  
582  
583  
584  
585  
586  
587  
588  
589  
590  
591  
592  
593  
594  
595  
596  
597  
598  
599  
600  
601  
602  
603  
604  
605  
606  
607  
608  
609  
610  
611  
612  
613  
614  
615  
616  
617  
618  
619  
620  
621  
622  
623  
624  
625  
626  
627  
628  
629  
630  
631  
632  
633  
634  
635  
636  
637  
638  
639  
640  
641  
642  
643  
644  
645  
646  
647  
648  
649  
650  
651  
652  
653  
654  
655  
656  
657  
658  
659  
660  
661  
662  
663  
664  
665  
666  
667  
668  
669  
670  
671  
672  
673  
674  
675  
676  
677  
678  
679  
680  
681  
682  
683  
684  
685  
686  
687  
688  
689  
690  
691  
692  
693  
694  
695  
696  
697  
698  
699  
700  
701  
702  
703  
704  
705  
706  
707  
708  
709  
710  
711  
712  
713  
714  
715  
716  
717  
718  
719  
720  
721  
722  
723  
724  
725  
726  
727  
728  
729  
730  
731  
732  
733  
734  
735  
736  
737  
738  
739  
740  
741  
742  
743  
744  
745  
746  
747  
748  
749  
750  
751  
752  
753  
754  
755  
756  
757  
758  
759  
7510  
7511  
7512  
7513  
7514  
7515  
7516  
7517  
7518  
7519  
7520  
7521  
7522  
7523  
7524  
7525  
7526  
7527  
7528  
7529  
7530  
7531  
7532  
7533  
7534  
7535  
7536  
7537  
7538  
7539  
7540  
7541  
7542  
7543  
7544  
7545  
7546  
7547  
7548  
7549  
7550  
7551  
7552  
7553  
7554  
7555  
7556  
7557  
7558  
7559  
7560  
7561  
7562  
7563  
7564  
7565  
7566  
7567  
7568  
7569  
7570  
7571  
7572  
7573  
7574  
7575  
7576  
7577  
7578  
7579  
7580  
7581  
7582  
7583  
7584  
7585  
7586  
7587  
7588  
7589  
7590  
7591  
7592  
7593  
7594  
7595  
7596  
7597  
7598  
7599  
75100  
75101  
75102  
75103  
75104  
75105  
75106  
75107  
75108  
75109  
75110  
75111  
75112  
75113  
75114  
75115  
75116  
75117  
75118  
75119  
75120  
75121  
75122  
75123  
75124  
75125  
75126  
75127  
75128  
75129  
75130  
75131  
75132  
75133  
75134  
75135  
75136  
75137  
75138  
75139  
75140  
75141  
75142  
75143  
75144  
75145  
75146  
75147  
75148  
75149  
75150  
75151  
75152  
75153  
75154  
75155  
75156  
75157  
75158  
75159  
75160  
75161  
75162  
75163  
75164  
75165  
75166  
75167  
75168  
75169  
75170  
75171  
75172  
75173  
75174  
75175  
75176  
75177  
75178  
75179  
75180  
75181  
75182  
75183  
75184  
75185  
75186  
75187  
75188  
75189  
75190  
75191  
75192  
75193  
75194  
75195  
75196  
75197  
75198  
75199  
75200  
75201  
75202  
75203  
75204  
75205  
75206  
75207  
75208  
75209  
75210  
75211  
75212  
75213  
75214  
75215  
75216  
75217  
75218  
75219  
75220  
75221  
75222  
75223  
75224  
75225  
75226  
75227  
75228  
75229  
75230  
75231  
75232  
75233  
75234  
75235  
75236  
75237  
75238  
75239  
75240  
75241  
75242  
75243  
75244  
75245  
75246  
75247  
75248  
75249  
75250  
75251  
75252  
75253  
75254  
75255  
75256  
75257  
75258  
75259  
75260  
75261  
75262  
75263  
75264  
75265  
75266  
75267  
75268  
75269  
75270  
75271  
75272  
75273  
75274  
75275  
75276  
75277  
75278  
75279  
75280  
75281  
75282  
75283  
75284  
75285  
75286  
75287  
75288  
75289  
75290  
75291  
75292  
75293  
75294  
75295  
75296  
75297  
75298  
75299  
75300  
75301  
75302  
75303  
75304  
75305  
75306  
75307  
75308  
75309  
75310  
75311  
75312  
75313  
75314  
75315  
75316  
75317  
75318  
75319  
75320  
75321  
75322  
75323  
75324  
75325  
75326  
75327  
75328  
75329  
75330  
75331  
75332  
75333  
75334  
75335  
75336  
75337  
75338  
75339  
75340  
75341  
75342  
75343  
75344  
75345  
75346  
75347  
75348  
75349  
75350  
75351  
75352  
75353  
75354  
75355  
75356  
75357  
75358  
75359  
75360  
75361  
75362  
75363  
75364  
75365  
75366  
75367  
75368  
75369  
75370  
75371  
75372  
75373  
75374  
75375  
75376  
75377  
75378  
75379  
75380  
75381  
75382  
75383  
75384  
75385  
75386  
75387  
75388  
75389  
75390  
75391  
75392  
75393  
75394  
75395  
75396  
75397  
75398  
75399  
75400  
75401  
75402  
75403  
75404  
75405  
75406  
75407  
75408  
75409  
75410  
75411  
75412  
75413  
75414  
75415  
75416  
75417  
75418  
75419  
75420  
75421  
75422  
75423  
75424  
75425  
75426  
75427  
75428  
75429  
75430  
75431  
75432  
75433  
75434  
75435  
75436  
75437  
75438  
75439  
75440  
75441  
75442  
75443  
75444  
75445  
75446  
75447  
75448  
75449  
75450  
75451  
75452  
75453  
75454  
75455  
75456  
75457  
75458  
75459  
75460  
75461  
75462  
75463  
75464  
75465  
75466  
75467  
75468  
75469  
75470  
75471  
75472  
75473  
75474  
75475  
75476  
75477  
75478  
75479  
75480  
75481  
75482  
75483  
75484  
75485  
75486  
75487  
75488  
75489  
75490  
75491  
75492  
75493  
75494  
75495  
75496  
75497  
75498  
75499  
75500  
75501  
75502  
75503  
75504  
75505  
75506  
75507  
75508  
75509  
75510  
75511  
75512  
75513  
75514  
75515  
75516  
75517  
75518  
75519  
75520  
75521  
75522  
75523  
75524  
75525  
75526  
75527  
75528  
75529  
75530  
75531  
75532  
75533  
75534  
75535  
75536  
75537  
75538  
75539  
75540  
75541  
75542  
75543  
75544  
75545  
75546  
75547  
75548  
75549  
75550  
75551  
75552  
75553  
75554  
75555  
75556  
75557  
75558  
75559  
75560  
75561  
75562  
75563  
75564  
75565  
75566  
75567  
75568  
75569  
75570  
75571  
75572  
75573  
75574  
75575  
75576  
75577  
75578  
75579  
75580  
75581  
75582  
75583  
75584  
75585  
75586  
75587  
75588  
75589  
75590  
75591  
75592  
75593  
75594  
75595  
75596  
75597  
75598  
75599  
75600  
75601  
75602  
75603  
75604  
75605  
75606  
75607  
75608  
75609  
75610  
75611  
75612  
75613  
75614  
75615  
75616  
75617  
75618  
75619  
75620  
75621  
75622  
75623  
75624  
75625  
75626  
75627  
75628  
75629  
75630  
75631  
75632  
75633  
75634  
75635  
75636  
75637  
75638  
75639  
75640  
75641  
75642  
75643  
75644  
75645  
75646  
75647  
75648  
75649  
75650  
75651  
75652  
75653  
75654  
75655  
75656  
75657  
75658  
75659  
75660  
75661  
75662  
75663  
75664  
75665  
75666  
75667  
75668  
75669  
75670  
75671  
75672  
75673  
75674  
75675  
75676  
75677  
75678  
75679  
75680  
75681  
75682  
75683  
75684  
75685  
75686  
75687  
75688  
75689  
75690  
75691  
75692  
75693  
75694  
75695  
75696  
75697  
75698  
75699  
75700  
75701  
75702  
75703  
75704  
75705  
75706  
75707  
75708  
75709  
75710  
75711  
75712  
75713  
75714  
75715  
75716  
75717  
75718  
75719  
75720  
75721  
75722  
75723  
75724  
75725  
75726  
75727  
75728  
75729  
75730  
75731  
75732  
75733  
75734  
75735  
75736  
75737  
75738  
75739  
75740  
75741  
75742  
75743  
75744  
75745  
75746  
75747  
75748  
75749  
75750  
75751  
75752  
75753  
75754  
75755  
75756  
75757  
75758  
75759  
75760  
75761  
75762  
75763  
75764  
75765  
75766  
75767  
75768  
75769  
75770  
75771  
75772  
75773  
75774  
75775  
75776  
75777  
75778  
75779  
75780  
75781  
75782  
75783  
75784  
75785  
75786  
75787  
75788  
75789  
75790  
75791  
75792  
75793  
75794  
75795  
75796  
75797  
75798  
75799  
75800  
75801  
75802  
75803  
75804  
75805  
75806  
75807  
75808  
75809  
75810  
75811  
75812  
75813  
75814  
75815  
75816  
75817  
75818  
75819  
75820  
75821  
75822  
75823  
75824  
75825  
75826  
75827  
75828  
75829  
75830  
75831  
75832  
75833  
75834  
75835  
75836  
75837  
75838  
75839  
75840  
75841  
75842  
75843  
75844  
75845  
75846  
75847  
75848  
75849  
75850  
75851  
75852  
75853  
75854  
75855  
75856  
75857  
75858  
75859  
75860  
75861  
75862  
75863  
75864  
75865  
75866  
75867  
75868  
75869  
75870  
75871  
75872  
75873  
75874  
75875  
75876  
75877  
75878  
75879  
75880  
75881  
75882  
75883  
75884  
75885  
75886  
75887  
75888  
75889  
75890  
75891  
75892  
75893  
75894  
75895  
75896  
75897  
75898  
75899  
75900  
75901  
75902  
75903  
75904  
75905  
75906  
75907  
75908  
75909  
75910  
75911  
75912  
75913  
75914  
75915  
75916  
75917  
75918  
75919  
75920  
75921  
75922  
75923  
75924  
75925  
75926  
75927  
75928  
75929  
75930  
75931  
75932  
75933  
75934  
75935  
75936  
75937  
75938  
75939  
75940  
75941  
75942  
75943  
75944  
75945  
75946  
75947  
75948  
75949  
75950  
75951  
75952  
75953  
75954  
75955  
75956  
75957  
75958  
75959  
75960  
75961  
75962  
75963  
75964  
75965  
75966  
75967  
75968  
75969  
75970  
75971  
75972  
75973  
75974  
75975  
75976  
75977  
75978  
75979  
75980  
75981  
75982  
75983  
75984  
75985  
75986  
75987  
75988  
75989  
75990  
75991  
75992  
75993  
75994  
75995  
75996  
75997  
75998  
75999  
75100  
75101  
75102  
75103  
75104  
75105  
75106  
75107  
75108  
75109  
75110  
75111  
75112  
75113  
75114  
75115  
75116  
75117  
75118  
75119  
75120  
75121  
75122  
75123  
75124  
75125  
75126  
75127  
75128  
75129  
75130  
75131  
75132  
75133  
75134  
75135  
75136  
75137  
75138  
75139  
75140  
75141  
75142  
75143  
75144  
75145  
75146  
75147  
75148  
75149  
75150  
75151  
75152  
75153  
75154  
75155  
75156  
75157  
75158  
75159  
75160  
75161  
75162  
75163  
75164  
75165  
75166  
75167  
75168  
75169  
75170  
75171  
75172  
75173  
75174  
75175  
75176  
75177  
75178  
75179  
75180  
75181  
75182  
75183  
75184  
75185  
75186  
75187  
75188  
75189  
75190  
75191  
75192  
75193  
75194  
75195  
75196  
75197  
75198  
75199  
75200  
75201  
75202  
75203  
75204  
75205  
75206  
75207  
75208  
75209  
75210  
75211  
75212  
75213  
75214  
75215  
75216  
75217  
75218  
75219  
75220  
75221  
75222  
75223  
75224  
75225  
75226  
75227  
75228  
75229  
75230  
75231  
75232  
75233  
75234  
75235  
75236  
75237  
75238  
75239  
75240  
75241  
75242  
75243  
75244  
75245  
75246  
75247  
75248  
75249  
75250  
75251  
75252  
75253  
75254  
75255  
75256  
75257  
75258  
75259  
75260  
75261  
75262  
75263  
75264  
75265  
75266  
75267  
75268  
75269  
75270  
75271  
75272  
75273  
75274  
75275  
75276  
75277  
75278

518 The node's color material will switch color indicating that<sup>554</sup>  
 519 it is saved in the system based on the tagging feature. In<sup>555</sup>  
 520 the case of neurons, the main branches would be all den-<sup>556</sup>  
 521 drites, excluding any other features e.g., spines.<sup>557</sup>

- 522 • In the case of highly-detailed skeletons, one would en-<sup>558</sup>  
 523 counter duplicate nodes and edges, disconnected parts,<sup>559</sup>  
 524 loops, and out of track skeletonization. Neuroscientists<sup>560</sup>  
 525 tried to delete all defects through an iterative manual pro-<sup>561</sup>  
 526 cess.<sup>562</sup>
- 527 • The soma area should be clear from any branching so neu-<sup>564</sup>  
 528 roscientists "cleaned" these parts by deleting all branches<sup>565</sup>  
 529 and merging them into one.<sup>566</sup>

530 In last two columns of table 3, we show the proofreading<sup>568</sup>  
 531 outputs for all the considered cells. In general, domain scien-<sup>569</sup>  
 532 tists found the proofreading task comfortable and accurate, and<sup>570</sup>  
 533 they particularly appreciated the immersiveness of the system<sup>571</sup>  
 534 for checking features and recognizing defects. For comparison,<sup>572</sup>  
 535 we asked expert neuroscientists to perform skeleton cleaning<sup>573</sup>  
 536 by using the external tracing metaphor together with the wall<sup>574</sup>  
 537 display setup: timings recorded for Neuron1 (27m58s) and for<sup>575</sup>  
 538 Neuron2 (46m10s) provided us evidence that the monoscopic<sup>576</sup>  
 539 setup associated to the external interface is not comfortable for<sup>577</sup>  
 540 cleaning skeletons.<sup>578</sup>

541 *Discussion.* In general, one of the drawbacks of dealing with<sup>580</sup>  
 542 an immersive environment on long sessions (20 minutes and<sup>581</sup>  
 543 more), is the symptoms of cybersickness and fatigue. This<sup>582</sup>  
 544 happened also for our system, and, during the sessions, users<sup>583</sup>  
 545 needed to take breaks every 15 minutes when performing each<sup>584</sup>  
 546 task. To this end, the system allows for multiple saves across<sup>585</sup>  
 547 sessions, and the user can retrieve the file anytime and continue<sup>586</sup>  
 548 where he/she last stopped. From this point of view, users liked<sup>587</sup>  
 549 the display wall setup in case of cyberfatigue, since they could<sup>588</sup>  
 550 sit, and rest while still working on the task. As general im-<sup>589</sup>  
 551 pression, the system was considered very useful for both proof-<sup>590</sup>  
 552 reading/cleaning pre-exported skeletons, as well as for creating<sup>591</sup>  
 553 skeletons from scratch. In particular, neuroscientists trained

in neurite tracing found very effective how the tool automatically provides a centerline, without the hassle of having to place it manually. Although the process of creating skeletons from scratch in VR can be time-consuming, automatic tools can make a lot of mistakes, and the time saved on the manual tracing would be lost on the proofreading anyways. This largely balanced the costs/benefits of the two approaches. Several factors contributed to make the creation process time consuming, mainly technical. One factor involves the order of tracing the various branches. Specifically, in some cases, users started tracing from the soma and proceeded towards the tips, while in other cases they made the opposite choice, by starting from the tip of the most extended branch and tracing towards the soma. We also experienced that another source of error was the path-stabilizer, in cases where the user happened to release a node at a bifurcation spot. Since the path-stabilizer is based on the concept of ray-casting, users needed to take care of correctly keeping the VR controller within the walls of the cellular structure. Issues with the stabilizer were experienced also in cases when the cell's main branch has too many spines within close distance to each other. In such situations, neuroscientists sometimes preferred to disable the stabilizer and operate on a full-manual mode. In general, we noticed that most creation issues were alleviated as users gained experience with the system, and we think that performance should dramatically improve once users repeat the process for many cells, i.e., after further training and experience. From the quality point of view, neuroscientists were satisfied with skeletons generated from scratch in VR, since they appeared well-structured and represented precisely the biological structure of the cells, tailored accordingly to their experience and knowledge about cell morphology. Regarding the proofreading task, domain scientists performed very well in checking and editing all five skeletons. They experienced some problems only with the Astrocyte, which took around 25 minutes to be proofread and edited. This is due to the fact that astrocytes have very complicated branched structures (see Tab. 3), where main processes are very difficult to recognize at first sight even for expert domain scientists.

592 **7.2. User study**

593 The use of Virtual Reality in Neuroscience is still at its early  
 594 stages [55, 5], therefore the user studies for evaluating the per-  
 595 formance of Virtual Environments for editing tasks are cur-  
 596 rently designed almost from scratch, because of the lack of stan-  
 597 dardized guidelines [56]. In our case, we aimed to assess the  
 598 performance of the system for creating and modifying skele-  
 599 ton representations of brain cells. To this end, we involved 12  
 600 users with different level of experience, and we asked them to  
 601 perform specific tasks under different conditions. We measured  
 602 times and accuracy, and we assessed the fatigue and comfort  
 603 through NASA-TLX questionnaire [57]. In the following we  
 604 detail the design of the user study and the outcomes of evalua-  
 605 tion. The main goal of the study was to evaluate the effects of  
 606 HMD and wall display on system performance, and whether  
 607 users felt more comfortable with external or internal tracing  
 608 metaphor for editing purposes (see figure 8). The study took  
 609 place in the visualization lab facility of King Abdullah Uni-  
 610 versity of Science and Technology, and in the department of  
 611 Anatomy at University of Turin.

612 **Design and protocol.** Subjects were asked to perform various  
 613 partial tasks on the system, using HMD or Wall display, and us-  
 614 ing internal or external metaphor for editing operations. Specif-  
 615 ically, after a period for training and getting comfortable with  
 616 the various setups and tools, we asked users to edit the skeleton  
 617 of a brain cell in the following way:

- 618 • trace a full branch
- 619 • correct a branch by removing nodes and links.

620 The branches to be traced were chosen randomly from two  
 621 long dendritic processes of Neuron1 and Neuron2 (see fig-  
 622 ure 10). Before each task, the user was shown how the task  
 623 is performed and how the joystick controls are being operated.  
 624 They were given a few minutes to practice the task until they  
 625 were comfortable enough to go ahead and start their mission.  
 626 Water and refreshments were offered at all times during the  
 627 study. Equipment were wiped and cleaned thoroughly with an-  
 628 tibacterial wipes after each use.

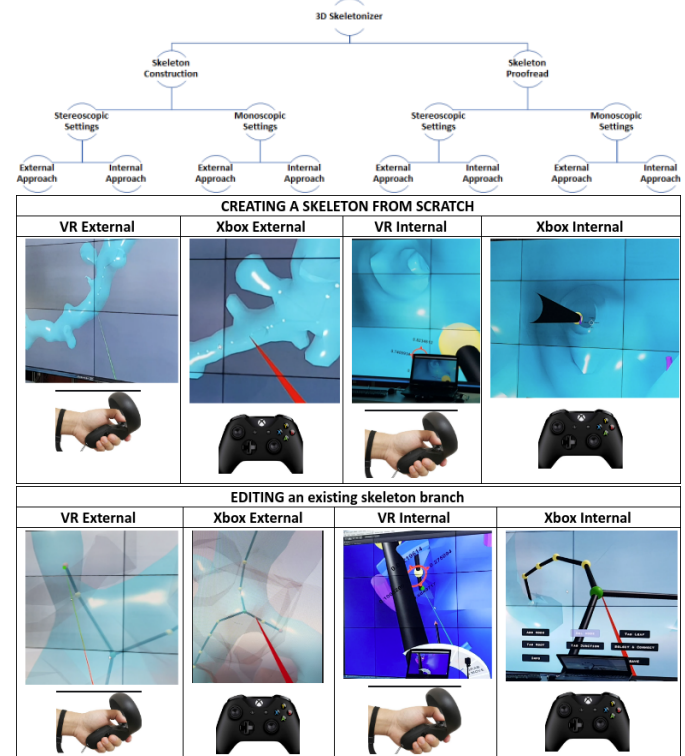


Fig. 9. User study protocol: subjects were asked to perform eight skeleton editing tasks under different conditions related to tracing metaphor and display setups.

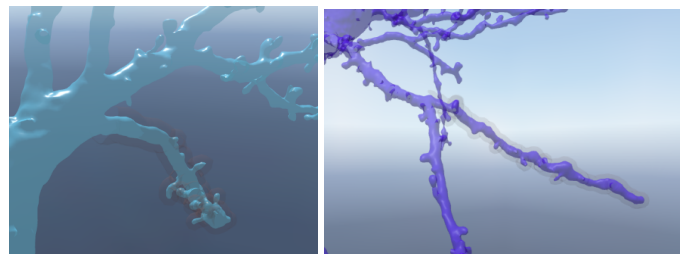
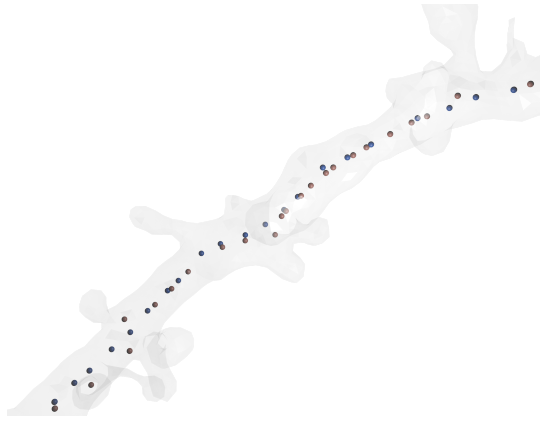


Fig. 10. User study data: subjects were asked to perform eight editing tasks under different conditions on two long processes from Neuron1 (left) and Neuron2 (right).

The two tasks were repeated randomly under different conditions, depending on the display type and the tracing metaphor for a total of 8 tasks (see fig. 9). Between each task a break of five minutes was given to subjects. After one task was complete (under the 4 conditions), users were asked to fill a 6 questions NASA-TLX form for comparing mental demand, physical demand, temporal demand, performance, effort and frustration (see table 6), with a 5 value Likert scale score ranging from low to high [57]. During the tasks we measured the total time for performing the tasks, and the paths of the traced branch. The tests were designed in a way that users did not need more than

640 60 minutes for training, completing all tasks, and filling the  
 641 forms. Think-out-loud comments were also recorded during  
 642 sessions.



**Fig. 11. Accuracy measurement.** We measure the accuracy of branch creation through Hausdorff distance between the ground truth branch computed by MCS [27] (in blue in this example), and the branch traced by subjects (in pink in this example).

643 *Quantitative performance.* For measuring performance in cre-  
 644 ation and editing tasks we compared branches obtained by users  
 645 with respect to ground truth obtained by MCS [27]. Figure 11  
 646 shows an example of a branch created by a user (in pink), and  
 647 the corresponding ground truth (in blue). Figure 12 shows  
 648 performance results for the tests related to accuracy for trace  
 649 branches and the completion time, obtained after filtering very  
 650 few outliers of subjects exhibiting really poor performance. We  
 651 show results in form of boxplots: the bottom and top of each  
 652 box are the first and third quartiles, the black line inside the box  
 653 is the second quartile (the median), and the ends of the whiskers  
 654 extending vertically from the boxes represent the lowest datum  
 655 still within 1.5 IQR (inter-quartile range) of the lower quartile,  
 656 and the highest datum still within 1.5 IQR of the upper quartile.  
 657 Outliers are indicated as small circles. On top we show the ac-  
 658 curacy of tracing in form of Hausdorff distance in  $\mu\text{m}$  between  
 659 the branch created by subjects and the ground-truth branch  
 660 computed through Mean Curvature Flow [27]: given two point  
 661 sets  $\mathbf{X}, \mathbf{Y}$  representing two branches, we measure the symmetric  
 662 Hausdorff distance [58] as the maximum of the asymmetric di-  
 663 rected Hausdorff distance  $H(\mathbf{X}, \mathbf{Y}) = \max(H(\mathbf{X}, \mathbf{Y}), H(\mathbf{Y}, \mathbf{X}))$ ,

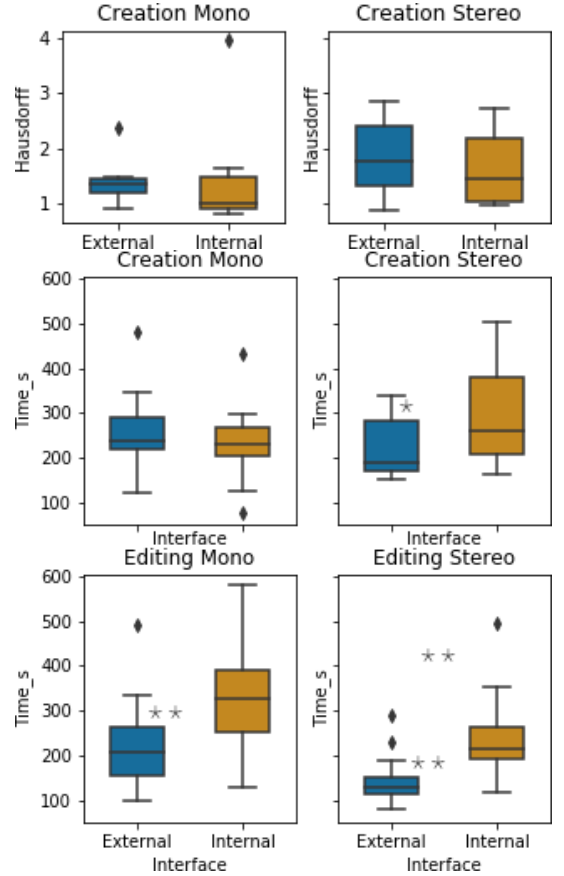


**Fig. 12. Quantitative performance.** Boxplots of accuracy performance for creation task (Hausdorff distance with respect to ground truth computed with Mean Curvature Flow in top row), and time performance for creation task (middle row) and editing task (bottom row). The bottom and top of each box are the first and third quartiles, the black line inside the box is the second quartile (the median), and the ends of the whiskers extending vertically from the boxes represent the lowest datum still within 1.5 IQR (inter-quartile range) of the lower quartile, and the highest datum still within 1.5 IQR of the upper quartile.

where the directed Hausdorff distance is defined as

$$\hat{H}(\mathbf{X}, \mathbf{Y}) = \max_{x \in \mathbf{X}} (\min_{y \in \mathbf{Y}} \|x - y\|). \quad (1)$$

ANOVA on the Hausdorff distance showed no effects due to the display for accuracy ( $1.49 \pm 0.88$  with Mono setup versus  $1.74 \pm 0.72$  with Stereo setup). Also the different interfaces do not appear to affect accuracy ( $1.63 \pm 0.65$  with External interface versus  $1.60 \pm 0.96$  with the Internal interface). On the bottom we compare the task completion time, either for the creation process (middle row) and the editing process (bottom row). ANOVA revealed an effect on interface when used with Stereo setup ( $p = 0.06$  with  $F = 3.893314$ ) for the creation task, with  $T = 218 \pm 64.6$ s for external interface, and  $T = 292 \pm 117.7$ s for internal interface, indicating that the external interface ap-

677 pears to be faster for creation especially in VR setup. Moreover,<sup>715</sup>  
 678 ANOVA revealed an important effect for editing either related<sup>716</sup>  
 679 to the display setup ( $p = 0.007$  with  $F = 8.106935$ ) and the<sup>717</sup>  
 680 interface ( $p = 0.001$  for  $F = 12.24$ ), indicating that external in-<sup>718</sup>  
 681 terface is perceived more comfortable and users perform editing<sup>719</sup>  
 682 tasks faster when they use the VR setup.<sup>720</sup>

683 *Qualitative performance.* Table 6 shows the questions and re-<sup>721</sup>  
 684 sults of NASA-TLX questionnaire proposed to subjects after<sup>722</sup>  
 685 tasks in order to evaluate their perception of performance, sat-<sup>723</sup>  
 686 isfaction, fatigue and stress under the different conditions.<sup>724</sup>

687 Figure 13 shows the boxplots of answers on a Likert scale<sup>725</sup>  
 688 (1=low,5=high). ANOVA on answers revealed a slight ef-<sup>726</sup>  
 689 fect for self satisfaction during the tracing task due to display<sup>727</sup>  
 690 setup ( $p = 0.03$  and  $F = 5.29$  for question Q4 in favor of VR<sup>728</sup>  
 691 setup), and effects on stress of display ( $p = 0.1$  and  $F = 2.81$ <sup>729</sup>  
 692 for question Q6 in favor of VR setup), and interface ( $F = 3.93$ <sup>730</sup>  
 693 and  $p = 0.05$  for question Q6 in favor of external tracing).<sup>731</sup>  
 694 With respect to the editing task, ANOVA revealed significant<sup>732</sup>  
 695 effects related to the display for mental demand ( $F = 12.67$  and<sup>733</sup>  
 696  $p = 0.001$  for question Q1 in favor of VR setup), physical de-<sup>734</sup>  
 697 mand ( $F = 12.86$  and  $p = 0.0008$  for question Q2 in favor of<sup>735</sup>  
 698 VR setup), fatigue ( $F = 8.14$  and  $p = 0.006$  for question Q5<sup>736</sup>  
 699 in favor of VR setup), and stress ( $f = 3.32$  and  $p = 0.07$  for<sup>737</sup>  
 700 question Q6 in favor of VR setup). No significant effects were<sup>738</sup>  
 701 found due to the different editing interface.<sup>739</sup>

702 *Discussion.* By observing the behavior of users with the sys-<sup>740</sup>  
 703 tem, we could note that the learning curve was rapid and the<sup>741</sup>  
 704 process per-se was pretty straight forward. In general, while<sup>742</sup>  
 705 performing the tasks, all operations required some time for the<sup>743</sup>  
 706 user to learn how to switch from one function to another one.<sup>744</sup>  
 707 To note also in this case the learning curve was pretty fast for<sup>745</sup>  
 708 experienced tracers. For the usage of the system on display<sup>746</sup>  
 709 wall setup, we realized that it is a factor of advantage if the user<sup>747</sup>  
 710 is a gamer, when using the XBOX controller: expert gamers  
 711 appeared to be more comfortable and to navigate blindly and<sup>748</sup>  
 712 effortlessly. In general the user study revealed that subjects feel<sup>749</sup>  
 713 more in control when in VR, since the orientation, navigation<sup>750</sup>  
 714 and interaction is more natural, and they can contribute with<sup>751</sup>

body, head and hands and not just two joysticks that restrict movement, eyesight and perspective. Since we designed the duration of tests in a way to do not let subjects perceive any problem of cybersickness (maximum 10 minutes for each task, and 5 minutes break between the tasks), results of the user study appear to be in contradiction with respect to the evaluation performed by expert users during the tracing of entire cells. It was a conscious decision during the design of the user study, even if we are aware that it would be important to evaluate the effects of cybersickness and to find ways to reduce it. We plan to carry out further user study investigations in future, with different task duration, in order to better evaluate the effects of cybersickness and physical efforts on our framework.

### 7.3. Case study: analysis of branch-based intracellular organelles.

One of the significant benefits of having skeleton representations of brain cells is the possibility of computing accurate measurements of morphological features. As a preliminary test, neuroscientists performed analysis of mitochondria, which are intracellular structures within the neural cells Neuron1 and Neuron2 (see Table 7). Since scientists are particularly interested in measuring specific geometric features of organelles, like lengths and radii (maximum, minimum, and average), adequate skeleton representations are needed for performing accurate measures. To this end, our system uses the same functionality equipped in the VR path stabilizer. Users can point at a particular node from a branch of interest, and the system uses the skeleton information for providing the measure of the full length, along with the radius values at each skeletal node contained in that branch. The measured values are shown as text labels in the scene on top of each node and recorded for subsequent statistical analysis (see fig. 14).

## 8. Conclusion

We presented an immersive system for creating, proofreading and exploring medial axis representations from highly detailed brain cellular morphologies reconstructed from serial electron microscopy. The framework is designed for stereoscopic HMD

Question	Results (Likert scale: 1=low 5=high)							
	Creation				Editing			
	Stereo		Mono		Stereo		Mono	
	External	Internal	External	Internal	External	Internal	External	Internal
<b>Q1:</b> How mentally demanding was it?	2.0 ± 0.7	2.4 ± 1.2	2.2 ± 0.9	2.7 ± 1.1	1.4 ± 0.5	1.8 ± 0.8	2.5 ± 1.1	2.7 ± 1.2
<b>Q2:</b> How physically demanding was it?	1.4 ± 0.7	2.0 ± 1.3	1.8 ± 0.9	1.7 ± 0.7	1.3 ± 0.5	1.6 ± 1.2	2.3 ± 1.1	2.3 ± 0.7
<b>Q3:</b> How hurried was the pace?	1.9 ± 0.8	2.2 ± 1.3	2.1 ± 1.2	2.3 ± 1.3	1.3 ± 0.5	1.5 ± 0.8	1.8 ± 1.2	1.9 ± 1.0
<b>Q4:</b> How successful were you?	4.3 ± 0.5	4.2 ± 0.7	3.8 ± 1.0	3.7 ± 1.0	4.4 ± 1.2	3.8 ± 1.5	3.9 ± 1.1	4.0 ± 1.1
<b>Q5:</b> How hard did you have to work ?	2.1 ± 0.8	2.3 ± 1.3	2.2 ± 0.8	2.7 ± 1.2	1.6 ± 0.7	2.2 ± 1.5	2.8 ± 1.4	3.0 ± 1.2
<b>Q6:</b> How stressed were you?	1.3 ± 0.5	1.7 ± 1.1	1.7 ± 1.0	2.3 ± 1.1	1.1 ± 0.3	1.6 ± 0.8	1.9 ± 1.0	1.7 ± 1.2

**Table 6.** User evaluation: 12 subjects were asked to compare two different editing metaphors (external and internal) on two different setups (Mono and Stereo) for two different tasks (creating and editing). Table shows the results of the answers of a 6-item questionnaire [?] on a Likert scale (1=low,5=high).

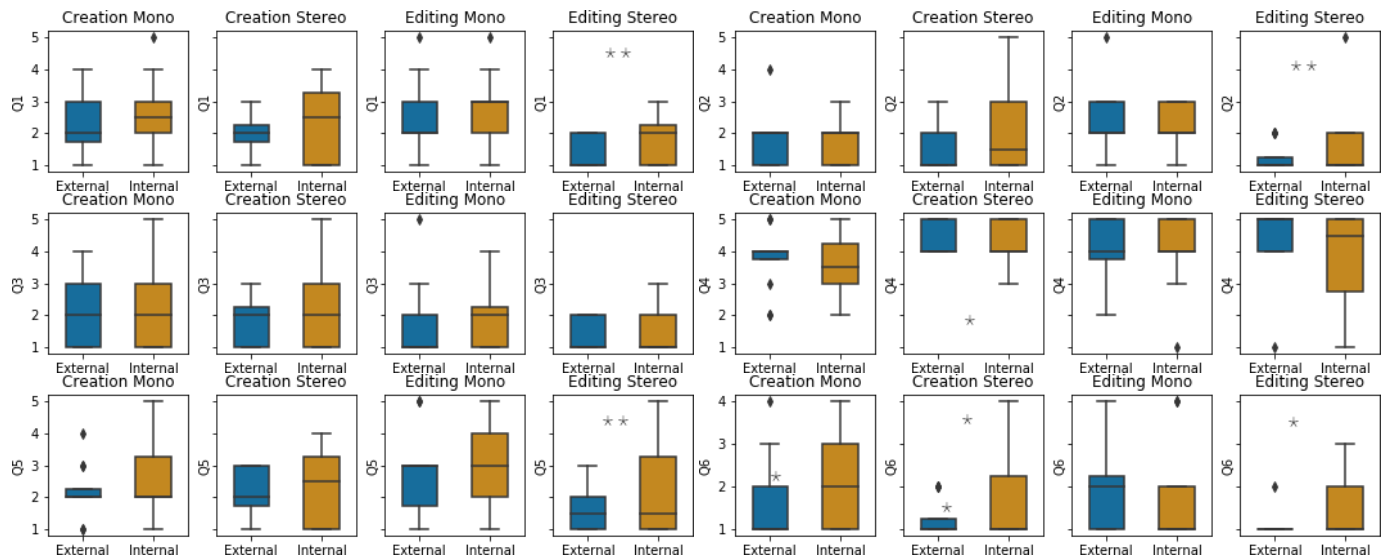


**Fig. 13.** Qualitative evaluation. Boxplots of answers in Likert scale for questions in table 6 for two different editing metaphors (external and internal), two different setups (Mono and Stereo), and two different tasks (creating and editing).. The bottom and top of each box are the first and third quartiles, the black line inside the box is the second quartile (the median), and the ends of the whiskers extending vertically from the boxes represent the lowest datum still within 1.5 IQR (inter-quartile range) of the lower quartile, and the highest datum still within 1.5 IQR of the upper quartile.

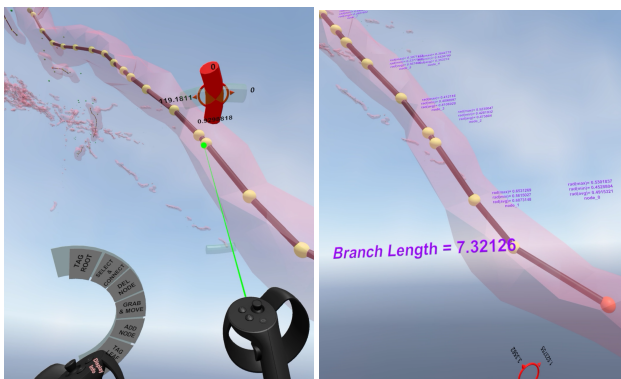


**Fig. 14.** Branch-based measurements. Our system performs calculations of measurements on intracellular structures. Left: User points the laser pointer at any node of a branch of interest to display node-relevant measurements. Right: Measurements of a mitochondrion branch are displayed.

Cell Name	Morphology	MC Skeleton	Nodes—Edges—Branches
Mito Neuron1			2,246— 1,963— 1,396
Mito Neuron2			1,749— 1,656— 811

**Table 7.** The intracellular structures of Neuron1 and Neuron2 showing mitochondria morphology, side by side with their skeletons generated via the MCS algorithm.

752 display setups and extended to large-scale monocular display<sup>790</sup>  
 753 in a way to alleviate unpleasant side-effects like cyber-sickness<sup>791</sup>  
 754 and fatigue, while still providing the ability to edit the skeleton<sup>792</sup>  
 755 in an immersive way. The system is currently used by neurosci-<sup>793</sup>  
 756 entists for deriving accurate skeleton representations to be used<sup>794</sup>  
 757 for classification, measurements, and simulation purposes [8].

758 We presented the outcomes of a user study to evaluate and com-<sup>795</sup>  
 759 pare the strengths the proposed system.

760 Our subjective preliminary evaluation showed that domain<sup>797</sup>  
 761 scientists feel particularly comfortable in using the system for<sup>798</sup>  
 762 proofreading and editing previously computed skeletons while<sup>800</sup>  
 763 they still consider the process of creating medial axis represen-<sup>801</sup>  
 764 tations from scratch to be comparable to automated or semi-<sup>802</sup>  
 765 automated 3D tools, in terms of time consumption, although<sup>803</sup>  
 766 they recognised how powerful the path stabilizer approach is to<sup>804</sup>  
 767 find the medial axis automatically, and the combination of ex-<sup>805</sup>  
 768 ternal and internal tracing metaphors dramatically speed-up the<sup>806</sup>  
 769 creation process. Plans to improve the system include the im-<sup>807</sup>  
 770 plementation of online collaborative schemes, in order to dis-<sup>808</sup>  
 771 tribute the creation process among multiple users, reduce the<sup>809</sup>  
 772 working time and effort, and at the same time increase the qual-<sup>810</sup>  
 773 ity of the output representation; and integration of visual ana-<sup>811</sup>  
 774 lytics tools for exploring feature distributions inside morpholo-<sup>812</sup>  
 775 gies [59] and tools for performing visual analysis of topolog-<sup>813</sup>  
 776 ical data representations associated to medial axis representa-<sup>814</sup>  
 777 tions [40]. Finally we customized the system for two differ-<sup>815</sup>  
 778 ent setups, considering direct metric interaction, and standard<sup>816</sup>  
 779 gaming indirect interfaces [54]. We did not yet investigate al-<sup>817</sup>  
 780 ternative interfaces that could speed-up the editing process and<sup>818</sup>  
 781 exploration, like touch-based systems to be attached to the dis-<sup>819</sup>  
 782 play wall setup or gesture recognition systems to be attached to<sup>820</sup>  
 783 the stereoscopic HMD setup. We plan to explore this avenue,<sup>821</sup>  
 784 in order to understand which interface is more performing for<sup>822</sup>  
 785 these kind of neuroscience investigations.<sup>823</sup>

## 786 9. Acknowledgement

787 This work is supported by KAUST King Abdullah<sup>850</sup>  
 788 University of Science and Technology KAUST-EPFL Al-<sup>851</sup>  
 789 liance for Integrative Modeling of Brain Energy Metabolism<sup>852</sup>

<sup>853</sup> https://www.kaust.edu.sa/en under KAUST CRG6 Grant No. 2313. We thank all the participants of the user study from KAUST and from the Neuroscience Institute "Cavalieri Ottolenghi". We also thank the anonymous reviewers for useful comments and suggestions.

## References

- [1] Calì, C, Agus, M, Kare, K, Boges, D, Lehväslaiho, H, Hadwiger, M, et al. 3D cellular reconstruction of cortical glia and parenchymal morphometric analysis from serial block-face electron microscopy of juvenile rat. *Progress in Neurobiology* 2019; To appear.
- [2] Coggan, JS, Keller, D, Calì, C, Lehväslaiho, H, Markram, H, Schürmann, F, et al. Norepinephrine stimulates glycogenolysis in astrocytes to fuel neurons with lactate. *PLoS computational biology* 2018;14(8):e1006392.
- [3] Markram, H, Müller, E, Ramaswamy, S, Reimann, M, Abdellah, M, Sanchez, C, et al. Reconstruction and simulation of neocortical microcircuitry. *Cell* 2015;163(2):456 – 492. URL: <http://www.sciencedirect.com/science/article/pii/S0092867415011915>. doi:<https://doi.org/10.1016/j.cell.2015.09.029>.
- [4] Calì, C, Baghabra, J, Boges, DJ, Holst, GR, Kreshuk, A, Hamprecht, FA, et al. Three-dimensional immersive virtual reality for studying cellular compartments in 3d models from EM preparations of neural tissues: 3d Virtual reality for neural tissue. *Journal of Comparative Neurology* 2016;524(1):23–38. URL: <http://doi.wiley.com/10.1002/cne.23852>. doi:10.1002/cne.23852.
- [5] Agus, M, Boges, D, Gagnon, N, Magistretti, PJ, Hadwiger, M, Calì, C. Glam: glycogen-derived lactate absorption map for visual analysis of dense and sparse surface reconstructions of rodent brain structures on desktop systems and virtual environments. *Computers & Graphics* 2018;74:85–98.
- [6] Usher, W, Klacansky, P, Federer, F, Bremer, PT, Knoll, A, Yarch, J, et al. A virtual reality visualization tool for neuron tracing. *IEEE transactions on visualization and computer graphics* 2017;24(1):994–1003.
- [7] Vezzoli, E, Calì, C, De Roo, M, Ponzoni, L, Sogne, E, Gagnon, N, et al. Ultrastructural evidence for a role of astrocytes and glycogen-derived lactate in learning-dependent synaptic stabilization. *Cerebral Cortex* 2019;.
- [8] Kanari, L, Ramaswamy, S, Shi, Y, Morand, S, Meystre, J, Perin, R, et al. Objective Morphological Classification of Neocortical Pyramidal Cells. *Cerebral Cortex* 2019;29(4):1719–1735. doi:10.1093/cercor/bhy339.
- [9] Longair, MH, Baker, DA, Armstrong, JD. Simple neurite tracer: open source software for reconstruction, visualization and analysis of neuronal processes. *Bioinformatics* 2011;27(17):2453–2454.
- [10] Schindelin, J, Arganda-Carreras, I, Frise, E, Kaynig, V, Longair, M, Pietzsch, T, et al. Fiji: an open-source platform for biological-image analysis. *Nature methods* 2012;9(7):676.
- [11] Schindelin, J, Rueden, CT, Hiner, MC, Eliceiri, KW. The imagej ecosystem: An open platform for biomedical image analysis. *Molecular reproduction and development* 2015;82(7-8):518–529.
- [12] Tagliasacchi, A, Delame, T, Spagnuolo, M, Amenta, N, Telea, A. 3d skeletons: A state-of-the-art report. In: Proceedings of the 37th Annual Conference of the European Association for Computer Graphics: State of the Art Reports. EG '16; Goslar Germany, Germany: Eurographics Association; 2016, p. 573–597. URL: <https://doi.org/10.1111/cgf.12865>. doi:10.1111/cgf.12865.
- [13] Boges, D, Calì, C, Magistretti, PJ, Hadwiger, M, Sicat, R, Agus, M. Immersive Environment for Creating, Proofreading, and Exploring Skeletons of Nanometric Scale Neural Structures. In: Agus, M, Corsini, M, Pintus, R, editors. Smart Tools and Apps for Graphics - Eurographics Italian Chapter Conference. The Eurographics Association. ISBN 978-3-03868-100-7; 2019, doi:10.2312/stag.20191360.
- [14] Mohammed, H, Al-Awami, A, Beyer, J, Calì, C, Magistretti, PJ, Pfister, H, et al. Abstractocyte: A Visual Tool for Exploring Nanoscale Astroglial Cell Morphology. *PacificVis*; 2017,.

- [15] Hadwiger, M, Al-Awami, A, Beyer, J, Agus, M, Pfister, H. SparseLeap:927 Efficient Empty Space Skipping for Large-Scale Volume Rendering. 2017;928
- [16] Keiriz, JJ, Zhan, L, Chukhman, M, Ajilore, O, Leow, AD, Forbes,929 AG. Exploring the human connectome topology in group studies. arXiv930 preprint arXiv:170610297 2017;. 931
- [17] Agus, M, Gobbetti, E, Iglesias Guitián, JA, Marton, F. Evaluating932 layout discrimination capabilities of continuous and discrete automulti-933 scopic displays. In: Proc. Fourth International Symposium on 3D Data934 Processing, Visualization and Transmission. 2010;. 935
- [18] Hänel, C, Pieperhoff, P, Hentschel, B, Amunts, K, Kuhlen, T. Inter-936 active 3d visualization of structural changes in the brain of a person with937 corticobasal syndrome. Frontiers in neuroinformatics 2014;8:42. 938
- [19] Laha, B, Sensharma, K, Schiffbauer, JD, Bowman, DA. Effects of939 immersion on visual analysis of volume data. IEEE Transactions on Vi-940 sualization and Computer Graphics 2012;18(4):597–606. 941
- [20] Agus, M, Gobbetti, E, Iglesias Guitián, J, Marton, F, Pintore, G.942 Gpu accelerated direct volume rendering on an interactive light field dis-943 play. Computer Graphics Forum 2008;27(3):231–240. Proc. Eurograph-944 ics 2008. 945
- [21] Laha, B, Bowman, DA, Socha, JJ. Effects of vr system fidelity on946 analyzing isosurface visualization of volume datasets. IEEE Transactions947 on Visualization and Computer Graphics 2014;20(4):513–522. 948
- [22] Forsberg, A, Katzourin, M, Wharton, K, Slater, M, et al. A compar-949 ative study of desktop, fishtank, and cave systems for the exploration of950 volume rendered confocal data sets. IEEE Transactions on Visualization951 and Computer Graphics 2008;14(3):551–563. 952
- [23] Alper, B, Hollerer, T, Kuchera-Morin, J, Forbes, A. Stereoscopic high-953 lighting: 2d graph visualization on stereo displays. IEEE Transactions on954 Visualization and Computer Graphics 2011;17(12):2325–2333. 955
- [24] Arsiwalla, XD, Zucca, R, Betella, A, Martinez, E, Dalmazzo, D,956 Omedas, P, et al. Network dynamics with brainx3: a large-scale simula-957 tion of the human brain network with real-time interaction. Frontiers in958 neuroinformatics 2015;9:2. 959
- [25] Xu, R, Thomas, MM, Leow, A, Ajilore, OA, Forbes, AG. Tempocave:960 Visualizing dynamic connectome datasets to support cognitive behavioral961 therapy. In: 2019 IEEE Visualization Conference (VIS). IEEE; 2019, p.962 186–190. 963
- [26] Sobiecki, A, Jalba, A, Telea, A. Comparison of curve and surface skele-964 tonization methods for voxel shapes. Pattern Recogn Lett 2014;47:147–965 156. URL: <http://dx.doi.org/10.1016/j.patrec.2014.01.012>. 966 doi:10.1016/j.patrec.2014.01.012. 967
- [27] Tagliasacchi, A, Alhashim, I, Olson, M, Zhang, H. Mean curvature968 skeletons. Comput Graph Forum 2012;31(5):1735–1744. URL: <http://dx.doi.org/10.1111/j.1467-8659.2012.03178.x>. doi:10.1111/j.1467-8659.2012.03178.x. 969
- [28] Yan, Y, Sykes, K, Chambers, E, Letscher, D, Ju, T. Erosion thick-970 ness on medial axes of 3d shapes. ACM Trans Graph 2016;35(4):38:1–973 38:12. URL: <http://doi.acm.org/10.1145/2897824.2925938>. 974 doi:10.1145/2897824.2925938. 975
- [29] Livesu, M, Attene, M, Patané, G, Spagnuolo, M. Explicit cylindrical976 maps for general tubular shapes. Computer-Aided Design 2017;90:27–977 36. 978
- [30] Li, P, Wang, B, Sun, F, Guo, X, Zhang, C, Wang, W. Q-mat: Comput-979 ing medial axis transform by quadratic error minimization. ACM Trans980 Graph 2015;35(1):8:1–8:16. URL: <http://doi.acm.org/10.1145/2753755>. doi:10.1145/2753755. 982
- [31] Yan, Y, Letscher, D, Ju, T. Voxel cores: Efficient, ro-983 bust, and provably good approximation of 3d medial axes. ACM984 Trans Graph 2018;37(4):44:1–44:13. URL: <http://doi.acm.org/10.1145/3197517.3201396>. 986 doi:10.1145/3197517.3201396.
- [32] Sato, M, Bitter, I, Bender, MA, Kaufman, AE, Nakajima, M. Teasar:987 Tree-structure extraction algorithm for accurate and robust skeletons. In:988 Proceedings of the 8th Pacific Conference on Computer Graphics and989 Applications. PG '00; Washington, DC, USA: IEEE Computer Soci-990 ety. ISBN 0-7695-0868-5; 2000, p. 281–. URL: [http://dl.acm.org/citation.cfm?id=826029.826514](http://dl.acm.org/991 citation.cfm?id=826029.826514). 992
- [33] Westenberger, P. Avizo-3d visualization framework. In: Geoinformatics993 Conference. 2008, p. 1–11. 994
- [34] Gillette, TA, Ascoli, GA. Topological characterization of neuronal arbor995 morphology via sequence representation: I-motif analysis. BMC bioin-996 formatics 2015;16(1):216. 997
- [35] Gillette, TA, Hosseini, P, Ascoli, GA. Topological characterization of998 neuronal arbor morphology via sequence representation: II-global alignment. BMC bioinformatics 2015;16(1):209.
- [36] Li, Y, Wang, D, Ascoli, GA, Mitra, P, Wang, Y. Metrics for com-999 paring neuronal tree shapes based on persistent homology. PloS one2017;12(8):e0182184.
- [37] Batabyal, T, Acton, ST. Neurosol: Automated classification of neurons using the sorted laplacian of a graph. In: 2017 IEEE 14th International Symposium on Biomedical Imaging (ISBI 2017). IEEE; 2017, p. 397–400.
- [38] Batabyal, T, Acton, ST. Elastic path2path: Automated morphological classification of neurons by elastic path matching. In: 2018 25th IEEE International Conference on Image Processing (ICIP). 2018, p. 166–170. doi:10.1109/ICIP.2018.8451446.
- [39] Riihimäki, H, Chacholski, W, Theorell, J, Hillert, J, Ramanujam, R. A topological data analysis based classification method for multiple measurements. arXiv preprint arXiv:190402971 2019;.
- [40] Kanari, L, Dłotko, P, Scolamiero, M, Levi, R, Shillcock, J, Hess, K, et al. A topological representation of branching neuronal morphologies. Neuroinformatics 2018;16(1):3–13. doi:10.1007/s12021-017-9341-1.
- [41] Abdellah, M, Hernando, J, Eilemann, S, Lapere, S, Antille, N, Markram, H, et al. Neuromorphovis: a collaborative framework for analysis and visualization of neuronal morphology skeletons reconstructed from microscopy stacks. Bioinformatics 2018;34(13):i574–i582.
- [42] Titze, B, Genoud, C. Volume scanning electron microscopy for imaging biological ultrastructure. Biology of the Cell 2016;108(11):307–323. doi:10.1111/boc.201600024.
- [43] Lichtman, JW, Pfister, H, Shavit, N. The big data challenges of connectomics. Nature neuroscience 2014;17(11):1448–1454.
- [44] Coggan, JS, Cali, C, Keller, D, Agus, M, Boges, D, Abdellah, M, et al. A process for digitizing and simulating biologically realistic oligocellular networks demonstrated for the neuro-Glio-Vascular ensemble. Frontiers in Neuroscience 2018;12. doi:10.3389/fnins.2018.00664.
- [45] Sommer, C, Straehle, C, Köthe, U, Hamprecht, FA. Ilastik: Interactive learning and segmentation toolkit. In: 2011 IEEE international symposium on biomedical imaging: From nano to macro. IEEE; 2011, p. 230–233. doi:10.1109/ISBI.2011.5872394.
- [46] Cardona, A, Saalfeld, S, Schindelin, J, Arganda-Carreras, I, Preibisch, S, Longair, M, et al. Trakem2 software for neural circuit reconstruction. PloS one 2012;7(6):e38011. doi:10.1371/journal.pone.0038011.
- [47] Agus, M, Cali, C, Al-Awami, A, Gobbetti, E, Magistretti, P, Hadwiger, M. Interactive volumetric visual analysis of glycogen-derived energy absorption in nanometric brain structures. Computer Graphics Forum 2019;38(3):427–439.
- [48] Murray, JW. Building virtual reality with Unity and Steam VR. AK Peters/CRC Press; 2017.
- [49] Desai, PR, Desai, PN, Ajmera, KD, Mehta, K. A review paper on oculus rift-a virtual reality headset. arXiv preprint arXiv:14081173 2014;.
- [50] Dempsey, P. The teardown: Htc vive vr headset. Engineering & Technology 2016;11(7–8):80–81.
- [51] Hess, R. The essential Blender: guide to 3D creation with the open source suite Blender. No Starch Press; 2007.
- [52] Cignoni, P, Callieri, M, Corsini, M, Dellepiane, M, Ganovelli, F, Ranzuglia, G. Meshlab: an open-source mesh processing tool. In: Eurographics Italian chapter conference; vol. 2008. 2008, p. 129–136.
- [53] Maraj, C, Hurter, J, Ferrante, S, Horde, L, Carter, J, Murphy, S. Oculus rift versus htc vive: Usability assessment from a teleportation task. In: International Conference on Human-Computer Interaction. Springer; 2019, p. 247–257.
- [54] Mendes, D, Caputo, FM, Giachetti, A, Ferreira, A, Jorge, J. A survey on 3d virtual object manipulation: From the desktop to immersive virtual environments. In: Computer graphics forum; vol. 38. Wiley Online Library; 2019, p. 21–45.
- [55] Cali, C, Baghabra, J, Boges, DJ, Holst, GR, Kreshuk, A, Hamprecht, FA, et al. 3D immersive virtual reality for studying cellular compartments in 3D models from EM preparations of neural tissues. Journal of Comparative Neurology 2016;524(1):23–38.
- [56] Jaeger, S, Klein, K, Joos, L, Zagermann, J, de Ridder, M, Kim, J, et al. Challenges for brain data analysis in vr environments. In: 2019 IEEE Pacific Visualization Symposium (PacificVis). IEEE; 2019, p. 42–46.
- [57] Hart, SG. Nasa-task load index (nasa-tlx); 20 years later. In: Proceedings

- 999 of the human factors and ergonomics society annual meeting; vol. 50.  
1000 Sage Publications Sage CA: Los Angeles, CA; 2006, p. 904–908.
- 1001 [58] Taha, AA, Hanbury, A. An efficient algorithm for calculating the exact  
1002 hausdorff distance. *IEEE transactions on pattern analysis and machine  
1003 intelligence* 2015;37(11):2153–2163.
- 1004 [59] Sicat, R, Li, J, Choi, J, Cordeil, M, Jeong, WK, Bach, B, et al. Dxr: A  
1005 toolkit for building immersive data visualizations. *IEEE transactions on  
1006 visualization and computer graphics* 2018;25(1):715–725.